The 2010 IEEE/RSJ International Conference on
Intelligent Robots and Systems
October 18-22, 2010, Taipei, Taiwan

A simplified model of planar snake robot locomotion

Pål Liljebäck, Kristin Y. Pettersen, Øyvind Stavdahl, and Jan Tommy Gravdahl

***Abstract*— This paper presents a model of the kinematics and dynamics of a planar, wheelless snake robot aimed at control design and stability analysis purposes. The proposed model is significantly less complex than existing models of planar snake robot locomotion. The paper presents an analysis of an existing complex snake robot model which reveals a set of essential properties that characterize the overall motion of a planar snake robot. The proposed model is developed to capture only these essential properties of snake locomotion, thereby significantly reducing the complexity compared to the original model used in the analysis. The paper presents simulation results that indicate that the *qualitative* behaviour of the proposed model and the original complex model are similar, and that a *quantitative* similarity is achieved with a proper choice of numerical values of the friction coefficients in the two models.**

I. Introduction

Inspired by biological snakes, snake robots carry the potential of meeting the growing need for robotic mobility in challenging environments. Snake robots consist of serially connected modules capable of bending in one or more planes. The many degrees of freedom of snake robots make them difficult to control, but provide traversability in irregular environments that surpasses the mobility of the more conventional wheeled, tracked and legged forms of robotic mobility.

Research on snake robots has been conducted for several decades and several models have been proposed to facilitate a better understanding of snake locomotion. Gray [1] conducted empirical and analytical studies of snake locomotion already in the 1940s. Hirose [2] studied biological snakes and developed mathematical relationships characterizing their motion, such as the *serpenoid curve*. Several models of wheelless snake robots influenced by ground friction have been developed [3]–[11]. All these models are, however, rather complex and thereby challenging to investigate analytically. An interesting exception is the work by Nilsson [12], which proposes and analyses a simplified model of the forward velocity of a planar snake robot based on energy arguments. In the authors' opinion, our understanding of snake locomotion so far is for the most part based on empirical studies of biological snakes and simulation-based synthesis of relationships between parameters of the snake. This is due to the complexity of existing models of snake locomotion.

Affiliation of Pål Liljebäck is shared between the Department of Engineering Cybernetics at the Norwegian University of Science and Technology, NO-7491 Trondheim, Norway, and SINTEF ICT, Dept. of Applied Cybernetics, N-7465 Trondheim, Norway. E-mail: Pal.Liljeback@sintef.no

K. Y. Pettersen, Øyvind Stavdahl, and Jan Tommy Gravdahl are with the Department of Engineering Cybernetics at the Norwegian University of Science and Technology, NO-7491 Trondheim, Norway. E-mail: {Kristin.Y.Pettersen, Oyvind.Stavdahl, Tommy.Gravdahl}@itk.ntnu.no

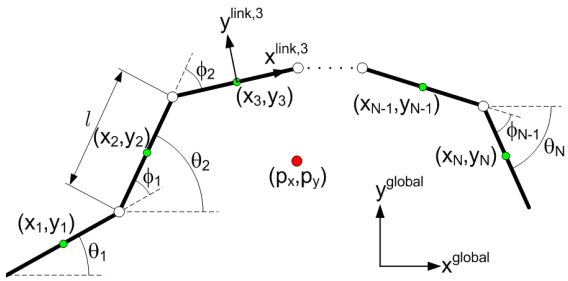

Fig. 1. Kinematic parameters for the snake robot.

This paper has two contributions. The first contribution is an analysis of an existing complex model of a planar snake robot that identifies a set of essential properties of snake locomotion. This analysis forms the basis of the second contribution, which is a *simplified model* of planar snake locomotion aimed at simplifying *analytical* investigations of the equations of motion. The proposed model is also developed to facilitate synthesis of new control strategies for snake robots. The basic idea behind the modelling approach is to capture only the essential part of the snake robot dynamics, i.e. the features that determine the overall behaviour of the snake.

The paper is organized as follows. Section II presents an existing complex model of a snake robot. Section III analyses the complex model in order to identify fundamental properties of snake locomotion. Section IV presents the simplified model of a snake robot. Section V presents a controller for the robot. Section VI presents simulation results. Finally, Section VII presents concluding remarks.

II. A complex model of a planar snake robot

This section summarizes an existing complex model of a planar snake robot previously presented in [11]. The model will be analysed in Section III in order to identify some essential properties of snake locomotion. This analysis will be used as a basis for the development of a simplified model of a planar snake robot in Section IV.

A. Kinematics of the snake robot

We consider a planar snake robot consisting of N links of length l interconnected by $N-1$ active joints. The kinematics of the robot is defined in terms of the symbols illustrated in Fig. 1. All N links have the same mass m and moment of inertia J. The total mass of the robot is therefore Nm. The mass of each link is uniformly distributed so that the link CM (center of mass) is located at its center point.

The snake robot moves in the horizontal plane and has a total of $N+2$ degrees of freedom. The CM (center of mass)

position of the robot is denoted by $\boldsymbol{p} = (p_x, p_y) \in \mathbb{R}^2$. The absolute angle θ_i of link i is expressed with respect to the global x axis with counterclockwise positive direction. As seen in Fig. 1, the relative angle between link i and link $i+1$ is given by $\phi_i = \theta_{i+1} - \theta_i$. The local coordinate system of each link is fixed in the CM of the link with x (tangential) and y (normal) axis oriented such that they are oriented in the directions of the global x and y axis, respectively, when the link angle is zero.

B. Equations of motion

We employ a *viscous* ground friction model in this study. Alternatively, we could have used a *Coulomb* friction model. However, we conjecture that a viscous and a Coulomb friction model are very similar from a control perspective when the friction is *anisotropic*. The work in e.g. [6] supports this conjecture. Moreover, viscous friction leads to simpler equations of motion compared to Coulomb friction. This greatly simplifies the analysis in Section III.

Under *anisotropic* friction conditions, a link has two viscous friction coefficients, c_t and c_n, describing the friction force in the tangential (along link x axis) and normal (along link y axis) direction of the link, respectively. As shown in [11], the friction force on link i, denoted by $\boldsymbol{f}_i \in \mathbb{R}^2$, can be written in terms of the link velocity, $\dot{x}_i$ and $\dot{y}_i$, as

$$\boldsymbol{f}_i = \begin{bmatrix} f_{x,i} \\ f_{y,i} \end{bmatrix} = - \begin{bmatrix} F_x(\theta_i) & F_{xy}(\theta_i) \\ F_{xy}(\theta_i) & F_y(\theta_i) \end{bmatrix} \begin{bmatrix} \dot{x}_i \\ \dot{y}_i \end{bmatrix} \tag{1}$$

where

$$F_x(\theta_i) = c_t \cos^2\theta_i + c_n \sin^2\theta_i \tag{2a}$$
$$F_{xy}(\theta_i) = (c_t - c_n)\sin\theta_i \cos\theta_i \tag{2b}$$
$$F_y(\theta_i) = c_t \sin^2\theta_i + c_n \cos^2\theta_i \tag{2c}$$

It is shown in [11] that the equations of motion of the snake robot in terms of the joint angles, $\boldsymbol{\phi} \in \mathbb{R}^{N-1}$, the absolute link angle of the head link, $\theta_N \in \mathbb{R}$, the position of the CM of the snake robot, $\boldsymbol{p} = (p_x, p_y) \in \mathbb{R}^2$, and the joint torques, $\boldsymbol{u} \in \mathbb{R}^{N-1}$, can be written as

$$\ddot{\boldsymbol{\phi}} = \boldsymbol{u} \tag{3a}$$
$$\ddot{\theta}_N = g(\boldsymbol{\phi}, \theta_N, \dot{\boldsymbol{\phi}}, \dot{\theta}_N, \dot{p}_x, \dot{p}_y, \boldsymbol{u}) \tag{3b}$$
$$Nm\ddot{p}_x = \sum_{i=1}^{N} f_{x,i} \tag{3c}$$
$$Nm\ddot{p}_y = \sum_{i=1}^{N} f_{y,i} \tag{3d}$$

where $g(\boldsymbol{\phi}, \theta_N, \dot{\boldsymbol{\phi}}, \dot{\theta}_N, \dot{p}_x, \dot{p}_y, \boldsymbol{u}) \in \mathbb{R}$ is a function of the state vector and the joint torques. The model of snake locomotion given by (3) will not be detailed further here, but we note that the model is extremely complex from a stability analysis perspective. This complexity is the main motivation behind the simplified model developed in Section IV.

III. Analysis of the Complex Model

This section analyses the complex model given by (3) in order to identify a set of properties that characterize the motion of a planar snake robot. These properties will be used as a basis for the development of a simplified model of a planar snake robot in Section IV.

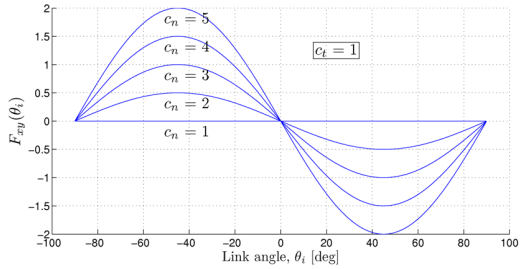

Fig. 2. The mapping from sideways link motion to forward propulsion for different viscous friction coefficients.

A. Analysis of propulsive forces during snake locomotion

This section investigates how a snake robot described by (3) is able to propel itself forward. We assume that the forward direction of motion is along the global positive x axis. The total force propelling the CM (center of mass) of the robot forward is therefore given from (3c) as

$$Nm\ddot{p}_x = \sum_{i=1}^{N} f_{x,i} \tag{4}$$

Wee see that the total *propulsive force* on the snake robot is simply the sum of all external forces in the global x direction. Inserting the expression for $f_{x,i}$ from (1) gives

$$Nm\ddot{p}_x = -\sum_{i=1}^{N} F_x(\theta_i)\dot{x}_i - \sum_{i=1}^{N} F_{xy}(\theta_i)\dot{y}_i \tag{5}$$

It is seen from (5) that the total propulsive force consists of two components, i.e. one involving the linear velocities of the links in the *forward* direction of motion, $F_x(\theta_i)\dot{x}_i$ (since we assume that the forward direction is along the x axis), and one involving the linear velocities *normal* to the direction of motion, $F_{xy}(\theta_i)\dot{y}_i$. $F_x(\theta_i)$ is given by (2a) and is clearly always positive. Furthermore, we assume that $\dot{x}_i > 0$ when the snake robot is moving forward ($\dot{p}_x > 0$). Due to the minus signs in (5), this means that the component $F_x(\theta_i)\dot{x}_i$ is *not* contributing to the forward propulsion of the robot, but rather opposing it. This is also expected since the snake robot must naturally be subjected to a friction force in the opposite direction of the motion.

Any propulsive force on the snake robot must therefore be produced by the *sideways* motion of the links, i.e. the product $F_{xy}(\theta_i)\dot{y}_i$. A plot of $F_{xy}(\theta_i)$ for different values of the normal friction coefficient c_n, while keeping the tangential friction coefficient c_t fixed, is shown in Fig. 2. For each plot, the angle between the link and the forward direction, θ_i, is varied from $-90°$ to $90°$. The sideways motion of the links have no effect on the propulsive force on the snake robot when the friction coefficients are equal since this gives $F_{xy}(\theta_i) = 0$. However, when $c_n > c_t$, Fig. 2 reveals that $F_{xy}(\theta_i)$ is negative as long as θ_i is positive, and vice versa. With reference to (5), this means that the sideways motion of link i produces a positive contribution to the propulsion of the snake robot through the product $F_{xy}(\theta_i)\dot{y}_i$ as long as $\mathrm{sgn}(\theta_i) = \mathrm{sgn}(\dot{y}_i)$.

The function $F_{xy}(\theta_i)$ can be viewed as a mapping from link velocities normal to the direction of motion into force

components in the direction of motion. The extrema of $F_{xy}(\theta_i)$ occur at $\theta_i = \pm 45°$. This means that, for a given $\dot{y}_i$, a link produces its highest propulsive force when it forms an angle of $\pm 45°$ with the forward direction of motion.

The above analysis is summarized by the following properties of planar snake locomotion:

Property 1: For a snake robot described by (3) with $c_n > c_t$, forward propulsion is produced by the link velocity components that are normal to the forward direction.

Property 2: For a snake robot described by (3) with $c_n > c_t$, the propulsive force generated by the transversal motion of link i is positive as long as $\text{sgn}(\theta_i) = \text{sgn}(\dot{y}_i)$.

Property 3: For a snake robot described by (3) with $c_n > c_t$, the magnitude of the propulsive force produced by link i increases when $|\theta_i|$ increases as long as $|\theta_i| < 45°$.

Note that these results are general in the sense that no assumptions have been made regarding the actual motion pattern displayed by the snake robot.

B. Analysis of turning locomotion

Having determined in the previous subsection how propulsion is generally achieved with a snake robot, we now investigate how turning motion is achieved. We assume that the snake robot moves by *lateral undulation* with a *serpenoid curve* [2]. This is a gait pattern consisting of horizontal waves that are propagated backwards along the snake body from head to tail. This is also the gait pattern most relevant for snake locomotion on flat surfaces. As proposed in [2], lateral undulation is achieved by controlling joint $i \in \{1, \cdots, N-1\}$ of the snake robot according to

$$\phi_{i,\text{ref}} = \alpha \sin(\omega t + (i-1)\delta) + \phi_o \tag{6}$$

where α and ω are the amplitude and frequency, respectively, of the sinusoidal joint motion and δ determines the phase shift between the joints. The parameter ϕ_o is a joint angle offset value that controls the overall direction of the locomotion. The effect of this parameter is illustrated in Fig. 3, which shows the result of a simulation of a snake robot described by (3) with $N = 10$ links of length $l = 0.14$ m. The top of Fig. 3 shows the trace of the head during the motion, while the bottom of the figure shows the average joint angle, which is defined as $\overline{\phi} = \frac{1}{N-1}\sum_{i=1}^{N-1}\phi_i$. The snake robot is controlled according to (6) with $\alpha = 30°$, $\omega = 70°/s$, and $\delta = 40°$. The offset angle is set to $\phi_o = 5°$ in the time interval $t \in [20, 30]$ and $\phi_o = -10°$ in the time interval $t \in [50, 60]$. The triangles pointing up and down in the top of Fig. 3 indicate, respectively, the beginning and end of these two time intervals. The offset angle is set to $\phi_o = 0°$ outside these two time intervals.

Fig. 3 shows that the snake robot crawls forward without turning as long as the average joint angle, $\overline{\phi}$, is zero. However, when the average joint angle is non-zero, the direction of the motion changes. We see from the figure that a positive (resp. negative) average joint angle produces a counterclockwise (resp. clockwise) rotation of the snake robot. We also see that the speed of the directional change is correlated with the amplitude of the average joint angle. This result is supported by the directional controllers for snake locomotion considered in e.g. [6], [13]. The following property summarizes this analysis:

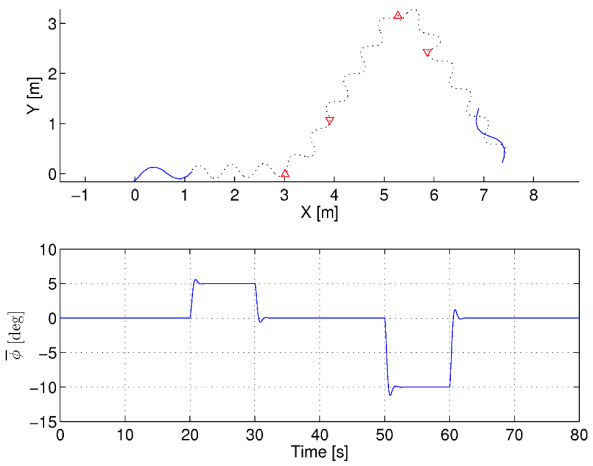

Fig. 3. Simulated motion of a snake robot with $N = 10$ links. A joint offset angle of $\phi_o = 5°$ and $\phi_o = -10°$ is introduced at $t = 20$ s and $t = 50$ s, respectively. Top: Trace of the head of the snake robot. Bottom: The average joint angle.

Property 4: During *lateral undulation* with a snake robot described by (3) with $c_n > c_t$, the overall direction of the locomotion remains constant as long as the average joint angle is zero, but will change in the counterclockwise (resp. clockwise) direction when the average joint angle is positive (resp. negative). The amplitude of the average joint angle determines how fast the direction of the locomotion changes.

C. Analysis of link motion during snake locomotion

From the results of the two previous subsections, it should be clear that planar snake locomotion consists of periodic body shape changes that generate external forces that propel the snake forward. These body shape changes can be characterized in terms of the joint angles $\phi_i = \theta_{i+1} - \theta_i$ defined in Section II-A. From Property 1, we know that the forward motion is induced by the motion of the links *normal* to the forward direction. This result led the authors to wonder if the body shape changes can be characterized in terms of the translational displacements of the links instead of the rotational joint motion. The motivation behind this idea is that translational motion is generally less complex to model than rotational motion. In particular, the model given by (3), which describes the rotational link motion of a snake robot, is quite complex.

To elaborate this idea further, the motion of a snake robot described by (3) with $N = 10$ links of length $l = 0.14$ m is shown in the top of Fig. 4. The robot conducts lateral undulation along the global x axis in accordance with (6) with $\alpha = 30°$, $\omega = 30°/s$, $\delta = 40°$, and $\phi_o = 0°$. The two bottom plots in Fig. 4 show the relative displacement between the CM (center of mass) of two arbitrarily chosen links (link 4 and link 5) in the global x and y direction, respectively. The plots indicate that, during lateral undulation, the relative displacement between the CM of two adjacent links along the forward direction of motion is approximately constant, while the relative displacement normal to the direction of motion oscillates around zero. This observation is an important basis for the modelling approach described in Section IV and is summarized as follows:

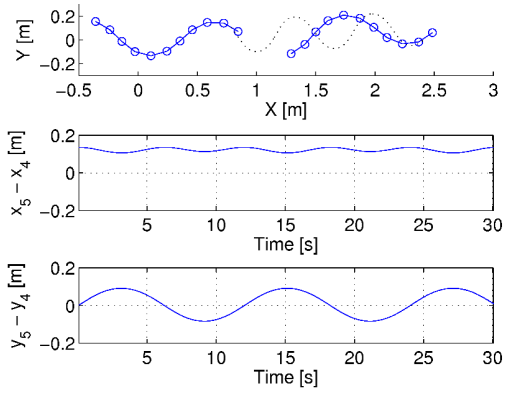

Fig. 4. Top: Simulated motion of a snake robot with $N = 10$ links. Middle: Relative displacement between the CM of link 4 and link 5 in the global x direction. Bottom: Relative displacement between the CM of link 4 and link 5 in the global y direction.

Property 5: The change in body shape during lateral undulation consists mainly of relative displacements of the CM of the links *normal* to the forward direction of motion. The relative displacements of the CM of the links along the forward direction are approximately constant.

IV. A SIMPLIFIED MODEL OF A PLANAR SNAKE ROBOT

In this section, we employ the results from the previous section in order to develop a simplified model of a planar snake robot. This model is intended for control design and stability analysis purposes.

A. Overview of the modelling approach

The idea behind the simplified model is illustrated in Fig. 5. The approach is basically to describe the body shape changes of a snake robot as *linear displacements* of the links with respect to each other instead of rotational displacements. From Property 5, we know that these linear displacements should be normal to the forward direction of motion. In addition, we know from Property 1 that these transversal displacements of the links are what propel the snake robot forward. This essentially means that we will model the revolute joints of a snake robot as prismatic (translational) joints. The rotational motion of the links during body shape changes will in other words be disregarded. However, the model will still capture the *effect* of the rotational link motion during body shape changes, which we know from Property 5 to be primarily a linear displacement of the CM of the links normal to the forward direction of motion.

The kinematics and dynamics of the snake robot will be detailed in the following subsections in terms of the symbols illustrated in Fig. 6 and Fig. 7. We will consider a planar snake robot with N links of length l interconnected by $N-1$ *prismatic* (translational) joints. All N links have the same mass m, and the total mass of the snake robot is thus Nm.

The following vectors and matrices are used in the development of the model:

$$\boldsymbol{A} = \begin{bmatrix} 1 & 1 & & \\ & \ddots & \ddots & \\ & & 1 & 1 \end{bmatrix}, \boldsymbol{D} = \begin{bmatrix} 1 & -1 & & \\ & \ddots & \ddots & \\ & & 1 & -1 \end{bmatrix}$$

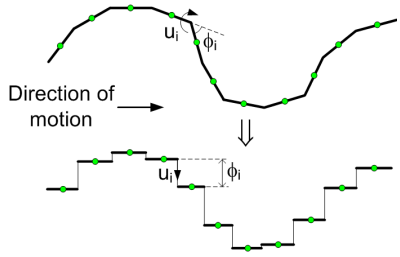

Fig. 5. The revolute joints of the snake robot are modelled as prismatic joints that displace the CM of each link transversal to the direction of motion.

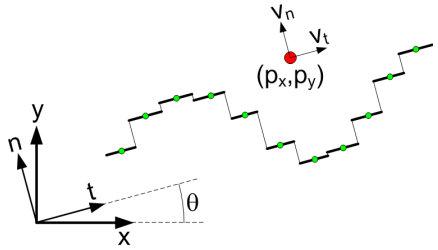

Fig. 6. Illustration of the two coordinate frames employed in the simplified model. The global x-y frame is fixed. The t-n frame is always aligned with the snake robot.

where $\boldsymbol{A} \in \mathbb{R}^{(N-1)\times N}$ and $\boldsymbol{D} \in \mathbb{R}^{(N-1)\times N}$. Furthermore, $\boldsymbol{e} = \begin{bmatrix} 1 & . & . & 1 \end{bmatrix}^T \in \mathbb{R}^N$, $\overline{\boldsymbol{e}} = \begin{bmatrix} 1 & . & . & 1 \end{bmatrix}^T \in \mathbb{R}^{N-1}$, $\overline{\boldsymbol{D}} = \boldsymbol{D}^T \left(\boldsymbol{D}\boldsymbol{D}^T \right)^{-1} \in \mathbb{R}^{N\times(N-1)}$.

We will use subscript i to denote element i of a vector. When parameters of the snake robot links are assembled into a vector, we associate element i of this vector with link i.

B. Kinematics of the snake robot

The snake robot moves in the horizontal plane and has a total of $N+2$ degrees of freedom. We define the motion of the robot with respect to the two coordinate frames illustrated in Fig. 6. The x-y frame is the fixed global frame. The t-n frame is always aligned with the snake robot, i.e. the t and n axis always point in the *tangential* and *normal* direction of the robot, respectively. The origin of both frames are fixed and coincide. We will denote the direction of the t axis as the *tangential* or *forward* direction of the robot, and the direction of the n axis as the *normal* direction. Note that we do not refer to the t-n frame as the *body* frame

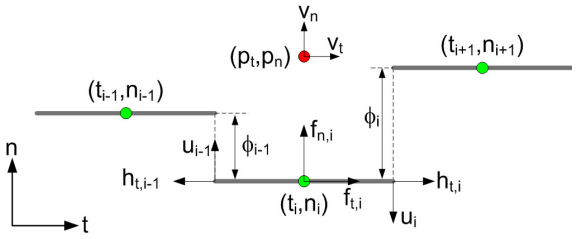

Fig. 7. Symbols characterizing the kinematics and dynamics of the snake robot.

of the snake robot since the t-n frame is not fixed to the robot. However, if a body frame fixed to the robot had been defined, the orientation of this frame would be identical to the orientation of the t-n frame.

The position of the snake robot is described through the coordinates of its CM (center of mass). As seen in Fig. 6 and Fig. 7, the global frame position of the robot is denoted by $(p_x, p_y) \in \mathbb{R}^2$, while the t-n frame position is denoted by $(p_t, p_n) \in \mathbb{R}^2$. The global frame orientation of the robot is denoted by $\theta \in \mathbb{R}$ and is expressed with respect to the global x axis with counterclockwise positive direction. The angle between the global x axis and the t axis is also θ since the t-n frame is always aligned with the robot. Describing the position in a frame which is always aligned with the snake robot is inspired by and similar to a coordinate transformation proposed in [14].

Remark 6: A snake robot with revolute joints, such as the robot described by (3), has no explicitly defined orientation. A common approach in previous literature has therefore been to describe the orientation of a snake robot as the mean of the absolute link angles [15], [16]. The present modelling approach avoids this issue since the scalar variable θ provides an explicit representation of the orientation of the snake robot.

The relationship between the t-n frame position and the global frame position is given by

$$p_t = p_x \cos\theta + p_y \sin\theta \tag{7a}$$
$$p_n = -p_x \sin\theta + p_y \cos\theta \tag{7b}$$

The forward and normal direction velocity of the CM of the snake robot, v_t and v_n, are illustrated in Fig. 6 and can be written as

$$v_t = \dot{p}_x \cos\theta + \dot{p}_y \sin\theta \tag{8a}$$
$$v_n = -\dot{p}_x \sin\theta + \dot{p}_y \cos\theta \tag{8b}$$

Differentiating (7) with respect to time and inserting (8) gives

$$\dot{p}_t = v_t + p_n \dot{\theta} \tag{9a}$$
$$\dot{p}_n = v_n - p_t \dot{\theta} \tag{9b}$$

We denote the t-n frame position of the CM of link i by $(t_i, n_i) \in \mathbb{R}^2$. The $N-1$ prismatic joints of the snake robot control the normal direction distance between the links. As seen in Fig. 7, the normal direction distance between link i and link $i+1$ is given by

$$\phi_i = n_{i+1} - n_i \tag{10}$$

and represents the coordinate of joint i. The controlled distance ϕ_i replaces the controlled joint angle in the original model given by (3). The link positions are constrained by the prismatic joints according to

$$t_i - t_{i+1} + l = 0 \tag{11a}$$
$$n_i - n_{i+1} + \phi_i = 0 \tag{11b}$$

These holonomic constraints may be expressed in matrix form for all links as

$$\boldsymbol{D}\boldsymbol{t} + l\overline{\boldsymbol{e}} = 0 \tag{12a}$$
$$\boldsymbol{D}\boldsymbol{n} + \boldsymbol{\phi} = 0 \tag{12b}$$

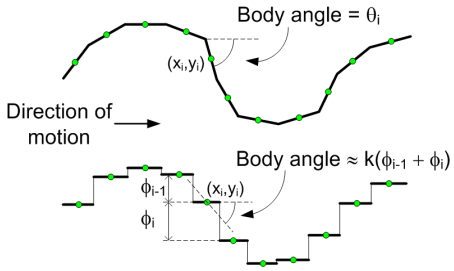

Fig. 8. The body angle of link i is θ_i for a snake robot with revolute joints. For a snake robot with prismatic joints, we can regard $\phi_{i-1} + \phi_i$ to be approximately proportional to the body angle with respect to the forward direction.

where $\boldsymbol{D}$ and $\overline{\boldsymbol{e}}$ are defined in Section IV-A, $\boldsymbol{t} = (t_1, \cdots, t_N) \in \mathbb{R}^N$, $\boldsymbol{n} = (n_1, \cdots, n_N) \in \mathbb{R}^N$, and $\boldsymbol{\phi} = (\phi_1, \cdots, \phi_{N-1}) \in \mathbb{R}^{N-1}$. The t-n frame position of the CM can be written in terms of the link positions as

$$p_t = \frac{1}{N}\boldsymbol{e}^T\boldsymbol{t} \tag{13a}$$
$$p_n = \frac{1}{N}\boldsymbol{e}^T\boldsymbol{n} \tag{13b}$$

where $\boldsymbol{e}$ is defined in Section IV-A. Combining (12a), (12b), (13a) and (13b) gives

$$\begin{bmatrix} \boldsymbol{D} \\ \frac{1}{N}\boldsymbol{e}^T \end{bmatrix}\boldsymbol{t} = \begin{bmatrix} -l\overline{\boldsymbol{e}} \\ p_t \end{bmatrix}, \quad \begin{bmatrix} \boldsymbol{D} \\ \frac{1}{N}\boldsymbol{e}^T \end{bmatrix}\boldsymbol{n} = \begin{bmatrix} -\boldsymbol{\phi} \\ p_n \end{bmatrix} \tag{14}$$

We can solve (14) for the link positions as

$$\boldsymbol{t} = p_t\boldsymbol{e} - l\overline{\boldsymbol{D}}\overline{\boldsymbol{e}} \tag{15a}$$
$$\boldsymbol{n} = p_n\boldsymbol{e} - \overline{\boldsymbol{D}}\boldsymbol{\phi} \tag{15b}$$

where $\overline{\boldsymbol{D}} = \boldsymbol{D}^T\left(\boldsymbol{D}\boldsymbol{D}^T\right)^{-1} \in \mathbb{R}^{N\times(N-1)}$. By differentiating (15a) and (15b) with respect to time and inserting (9a) and (9b), the individual link velocities are given as

$$\dot{\boldsymbol{t}} = \left(v_t + p_n\dot{\theta}\right)\boldsymbol{e} \tag{16a}$$
$$\dot{\boldsymbol{n}} = \left(v_n - p_t\dot{\theta}\right)\boldsymbol{e} - \overline{\boldsymbol{D}}\dot{\boldsymbol{\phi}} \tag{16b}$$

C. Ground friction model

We employ a viscous ground friction model similar to the friction model described in Section II-B. The ground friction forces, which act on the CM of each link, must be defined so that Property 1, Property 2, and Property 3 from Section III-A also apply to the simplifed model of the snake robot.

Property 1 requires that the normal direction velocity of link i, which is given by $\dot{n}_i$, produces a friction force component in the tangential direction. In order to preserve Property 3, we assume that the magnitude of this tangential friction force component is proportional to $\phi_{i-1} + \phi_i$, i.e. the relative distance between link $i-1$ and link $i+1$. This assumption is illustrated in Fig. 8, which shows that we can regard $\phi_{i-1}+\phi_i$ to be approximately proportional to the body angle with respect to the forward direction. Property 2 is preserved if the tangential friction force component produced by $\dot{n}_i$ is positive when $\operatorname{sgn}\left(\phi_{i-1} + \phi_i\right) = \operatorname{sgn}\left(\dot{n}_i\right)$ and negative otherwise.

We denote the tangential and normal direction friction force on link i by $f_{t,i}$ and $f_{n,i}$, respectively. The following friction model complies with the above requirements:

$$\begin{bmatrix} f_{t,i} \\ f_{n,i} \end{bmatrix} = \begin{bmatrix} -c_1 & c_2\left(\phi_{i-1}+\phi_i\right) \\ c_2\left(\phi_{i-1}+\phi_i\right) & -c_1 \end{bmatrix} \begin{bmatrix} \dot{t}_i \\ \dot{n}_i \end{bmatrix}_{\dot{\theta}=0} \tag{17}$$

The viscous friction coefficient c_1 determines the magnitude of the friction force components resisting the tangential and normal link motion, while c_2 determines the magnitude of the tangential and normal friction force components induced by the normal and tangential link velocities, respectively. The subscript $\dot{\theta}=0$ after the link velocity means that the friction model disregards the link velocity components due to the angular velocity of the snake robot, $\dot{\theta}$. This is a reasonable assumption since the dynamics of the angular rotation of the snake robot will generally be much slower than the body shape dynamics. This assumption also simplifies the friction model significantly. The friction forces on all N links can now be expressed as

$$\begin{bmatrix} \boldsymbol{f}_t \\ \boldsymbol{f}_n \end{bmatrix} = \begin{bmatrix} -c_1\boldsymbol{I}_N & c_2\operatorname{diag}\left(\boldsymbol{A}^T\boldsymbol{\phi}\right) \\ c_2\operatorname{diag}\left(\boldsymbol{A}^T\boldsymbol{\phi}\right) & -c_1\boldsymbol{I}_N \end{bmatrix} \begin{bmatrix} \dot{\boldsymbol{t}} \\ \dot{\boldsymbol{n}} \end{bmatrix}_{\dot{\theta}=0} \tag{18}$$

where $\boldsymbol{f}_t \in \mathbb{R}^N$ and $\boldsymbol{f}_n \in \mathbb{R}^N$ contain, respectively, the tangential and normal direction friction forces on the links, $\boldsymbol{I}_N$ is the $N \times N$ identity matrix, $\boldsymbol{A}$ is defined in Section IV-A, and the operator $\operatorname{diag}(\cdot)$ produces a diagonal matrix with the elements of its argument along its diagonal. Inserting (16a) and (16b) into (18) with $\dot{\theta}=0$ gives

$$\boldsymbol{f}_t = -c_1 v_t \boldsymbol{e} + c_2 \operatorname{diag}\left(\boldsymbol{A}^T\boldsymbol{\phi}\right)\left(v_n\boldsymbol{e} - \overline{\boldsymbol{D}}\dot{\boldsymbol{\phi}}\right) \tag{19a}$$

$$\boldsymbol{f}_n = -c_1 v_n \boldsymbol{e} + c_1\overline{\boldsymbol{D}}\dot{\boldsymbol{\phi}} + c_2 v_t \operatorname{diag}\left(\boldsymbol{A}^T\boldsymbol{\phi}\right)\boldsymbol{e} \tag{19b}$$

D. Dynamics of the snake robot

This section presents a model of the accelerations of the snake robot. From Fig. 7, it can be seen that the force balance for link i is given by

$$m\ddot{t}_i = f_{t,i} + h_{t,i} - h_{t,i-1} \tag{20a}$$

$$m\ddot{n}_i = f_{n,i} - u_i + u_{i-1} \tag{20b}$$

where $f_{t,i}$ and $f_{n,i}$ are the ground friction forces defined in (17), $h_{t,i}$ and $h_{t,i-1}$ are the joint constraint forces on link i from link $i+1$ and link $i-1$, respectively, and u_i and u_{i-1} are the actuator forces at joint i and joint $i-1$, respectively. The joint constraint forces, $h_{t,i}$ and $h_{t,i-1}$, prevent relative motion between the links in the tangential direction and the actuator forces, u_i and u_{i-1}, produce relative motion between the links in the normal direction. The force balance for all links can be written in matrix form as

$$m\ddot{\boldsymbol{t}} = \boldsymbol{f}_t + \boldsymbol{D}^T\boldsymbol{h}_t \tag{21a}$$

$$m\ddot{\boldsymbol{n}} = \boldsymbol{f}_n - \boldsymbol{D}^T\boldsymbol{u} \tag{21b}$$

where $\boldsymbol{D}$ is defined in Section IV-A, $\boldsymbol{h}_t = (h_{t,1}, \cdots, h_{t,N-1}) \in \mathbb{R}^{N-1}$, and $\boldsymbol{u} = (u_1, \cdots, u_{N-1}) \in \mathbb{R}^{N-1}$. Premultiplying (21b) by $\frac{1}{m}\boldsymbol{D}$ gives

$$\boldsymbol{D}\ddot{\boldsymbol{n}} = \frac{1}{m}\boldsymbol{D}\boldsymbol{f}_n - \frac{1}{m}\boldsymbol{D}\boldsymbol{D}^T\boldsymbol{u} \tag{22}$$

By differentiating (12b) twice with respect to time, it is easily seen that $\boldsymbol{D}\ddot{\boldsymbol{n}} = -\ddot{\boldsymbol{\phi}}$. We can therefore write the body shape dynamics of the snake robot as

$$\ddot{\boldsymbol{\phi}} = -\frac{1}{m}\boldsymbol{D}\boldsymbol{f}_n + \frac{1}{m}\boldsymbol{D}\boldsymbol{D}^T\boldsymbol{u} \tag{23}$$

Inserting (19b) into (23) and using the easily verifiable relations $\boldsymbol{D}\boldsymbol{e} = \boldsymbol{0}$, $\boldsymbol{D}\overline{\boldsymbol{D}} = \boldsymbol{I}_{N-1}$, and $\boldsymbol{D}\operatorname{diag}\left(\boldsymbol{A}^T\boldsymbol{\phi}\right)\boldsymbol{e} = -\boldsymbol{A}\boldsymbol{D}^T\boldsymbol{\phi}$, we get

$$\ddot{\boldsymbol{\phi}} = -\frac{c_1}{m}\dot{\boldsymbol{\phi}} + \frac{c_2}{m}v_t\boldsymbol{A}\boldsymbol{D}^T\boldsymbol{\phi} + \frac{1}{m}\boldsymbol{D}\boldsymbol{D}^T\boldsymbol{u} \tag{24}$$

The tangential and normal direction acceleration of the CM of the snake robot, denoted by $\dot{v}_t$ and $\dot{v}_n$, respectively, are given as the sum of all tangential and normal direction forces on the links divided by the mass of the snake robot, Nm. This is written

$$\dot{v}_t = \frac{1}{Nm}\left(\boldsymbol{e}^T m\ddot{\boldsymbol{t}}\right) = \frac{1}{Nm}\boldsymbol{e}^T\boldsymbol{f}_t \tag{25a}$$

$$\dot{v}_n = \frac{1}{Nm}\left(\boldsymbol{e}^T m\ddot{\boldsymbol{n}}\right) = \frac{1}{Nm}\boldsymbol{e}^T\boldsymbol{f}_n \tag{25b}$$

where we note that the joint constraint forces, $\boldsymbol{h}_t$, and the actuator forces, $\boldsymbol{u}$, are eliminated when the link accelerations are summed, i.e. $\boldsymbol{e}^T\boldsymbol{D}^T = \boldsymbol{0}$. Inserting (19a) and (19b) into (25a) and (25b), and using the easily verifiable relations $\boldsymbol{e}^T\operatorname{diag}\left(\boldsymbol{A}^T\boldsymbol{\phi}\right)\boldsymbol{e} = 2\overline{\boldsymbol{e}}^T\boldsymbol{\phi}$, $\boldsymbol{e}^T\overline{\boldsymbol{D}} = \boldsymbol{0}$, and $\boldsymbol{e}^T\operatorname{diag}\left(\boldsymbol{A}^T\boldsymbol{\phi}\right)\overline{\boldsymbol{D}} = \boldsymbol{\phi}^T\boldsymbol{A}\overline{\boldsymbol{D}}$, we get

$$\dot{v}_t = -\frac{c_1}{m}v_t + \frac{2c_2}{Nm}v_n\overline{\boldsymbol{e}}^T\boldsymbol{\phi} - \frac{c_2}{Nm}\boldsymbol{\phi}^T\boldsymbol{A}\overline{\boldsymbol{D}}\dot{\boldsymbol{\phi}} \tag{26a}$$

$$\dot{v}_n = -\frac{c_1}{m}v_n + \frac{2c_2}{Nm}v_t\overline{\boldsymbol{e}}^T\boldsymbol{\phi} \tag{26b}$$

As noted in Remark 6, a significant difference between the snake robot with revolute joints in (3) and the snake robot with prismatic joints in the simplified model concerns the absolute orientation of the robot. The snake robot with revolute joints has no explicitly defined orientation since there is an independent link angle associated with each link. The orientation of the robot with prismatic joints, however, is explicitly defined in terms of the scalar angle θ, which is also the angle of all the links. This difference must be taken into account when we model the angular acceleration, $\ddot{\theta}$, of the snake robot with prismatic joints. The model must comply with Property 4 from Section III-B, which basically requires that the direction of the forward motion (i.e. the orientation θ) changes when the average of the joint coordinates, $\frac{1}{N-1}\overline{\boldsymbol{e}}^T\boldsymbol{\phi}$, is nonzero. A model that complies with this property is

$$\ddot{\theta} = -c_3\dot{\theta} + \frac{c_4}{N-1}v_t\overline{\boldsymbol{e}}^T\boldsymbol{\phi} \tag{27}$$

The rotation of the snake robot is opposed by a viscous friction torque determined by the friction coefficient c_3. In addition, the average of the joint coordinates induces a torque on the robot which is scaled through the coefficient c_4 and also through the forward velocity v_t. The induced torque must be multiplied by v_t since the snake robot otherwise would experience a constant angular velocity when it is lying still with a nonzero average joint coordinate. Even though the model of $\ddot{\theta}$ is not based on first principles, the behaviour of

this model will closely resemble the behaviour of a snake robot with revolute joints when the coefficients c_3 and c_4 are properly chosen.

E. The complete simplified model of the snake robot

This section summarizes the complete model of a planar snake robot with N links of mass m. Since the robot has $N+2$ degrees of freedom, a state vector containing the generalized coordinates and velocities of the robot will have dimension $2N+4$. We choose the state vector as

$$\boldsymbol{x} = (\boldsymbol{\phi}, \theta, p_t, p_n, \boldsymbol{v}_\phi, v_\theta, v_t, v_n) \in \mathbb{R}^{2N+4} \tag{28}$$

where $\boldsymbol{\phi} \in \mathbb{R}^{N-1}$ are the joint coordinates, $\theta \in \mathbb{R}$ is the absolute orientation, $(p_t, p_n) \in \mathbb{R}^2$ is the t-n frame position of the CM, $\boldsymbol{v}_\phi = \dot{\boldsymbol{\phi}} \in \mathbb{R}^{N-1}$ are the joint velocities, $v_\theta = \dot{\theta} \in \mathbb{R}$ is the angular velocity, and $(v_t, v_n) \in \mathbb{R}^2$ is the tangential and normal direction velocity of the snake robot. From (9), (24), (26), and (27), we can write the complete model of the snake robot as

$$\dot{\boldsymbol{\phi}} = \boldsymbol{v}_\phi \tag{29a}$$
$$\dot{\theta} = v_\theta \tag{29b}$$
$$\dot{p}_t = v_t + p_n v_\theta \tag{29c}$$
$$\dot{p}_n = v_n - p_t v_\theta \tag{29d}$$
$$\dot{\boldsymbol{v}}_\phi = -\frac{c_1}{m}\boldsymbol{v}_\phi + \frac{c_2}{m} v_t \boldsymbol{A}\boldsymbol{D}^T\boldsymbol{\phi} + \frac{1}{m}\boldsymbol{D}\boldsymbol{D}^T\boldsymbol{u} \tag{29e}$$
$$\dot{v}_\theta = -c_3 v_\theta + \frac{c_4}{N-1} v_t \overline{\boldsymbol{e}}^T\boldsymbol{\phi} \tag{29f}$$
$$\dot{v}_t = -\frac{c_1}{m}v_t + \frac{2c_2}{Nm} v_n \overline{\boldsymbol{e}}^T\boldsymbol{\phi} - \frac{c_2}{Nm}\boldsymbol{\phi}^T\boldsymbol{A}\overline{\boldsymbol{D}}\boldsymbol{v}_\phi \tag{29g}$$
$$\dot{v}_n = -\frac{c_1}{m}v_n + \frac{2c_2}{Nm} v_t \overline{\boldsymbol{e}}^T\boldsymbol{\phi} \tag{29h}$$

where $\boldsymbol{u} \in \mathbb{R}^{N-1}$ are the actuator forces at the joints, $\boldsymbol{A}$, $\boldsymbol{D}$, $\overline{\boldsymbol{D}}$, and $\overline{\boldsymbol{e}}$ are defined in Section IV-A, and c_1, c_2, c_3 and c_4 are scalar constants characterizing the external forces acting on the snake robot.

V. Controller design

In this section, we propose a controller for the snake robot. Since $\boldsymbol{D}\boldsymbol{D}^T \in \mathbb{R}^{(N-1)\times(N-1)}$ in (29e) is a constant invertible matrix, we can linearize the dynamics of the joints with the following linearizing controller:

$$\boldsymbol{u} = m\left(\boldsymbol{D}\boldsymbol{D}^T\right)^{-1}\left(\overline{\boldsymbol{u}} + \frac{c_1}{m}\dot{\boldsymbol{\phi}} - \frac{c_2}{m} v_t \boldsymbol{A}\boldsymbol{D}^T\boldsymbol{\phi}\right) \tag{30}$$

where $\overline{\boldsymbol{u}} \in \mathbb{R}^{N-1}$ is a new set of control inputs. This controller transforms the joint dynamics (29e) into $\dot{\boldsymbol{v}}_\phi = \ddot{\boldsymbol{\phi}} = \overline{\boldsymbol{u}}$, which is identical to the joint dynamics of the snake robot with revolute joints in (3). We set $\overline{\boldsymbol{u}}$ according to the control law

$$\overline{\boldsymbol{u}} = \ddot{\boldsymbol{\phi}}_{\text{ref}} + k_d\left(\dot{\boldsymbol{\phi}}_{\text{ref}} - \dot{\boldsymbol{\phi}}\right) + k_p\left(\boldsymbol{\phi}_{\text{ref}} - \boldsymbol{\phi}\right) \tag{31}$$

where k_p and k_d are positive scalar controller gains and $\boldsymbol{\phi}_{\text{ref}} \in \mathbb{R}^{N-1}$ are the joint reference coordinates. The error dynamics of the joints is therefore given by

$$\left(\ddot{\boldsymbol{\phi}}_{\text{ref}} - \ddot{\boldsymbol{\phi}}\right) + k_d\left(\dot{\boldsymbol{\phi}}_{\text{ref}} - \dot{\boldsymbol{\phi}}\right) + k_p\left(\boldsymbol{\phi}_{\text{ref}} - \boldsymbol{\phi}\right) = 0 \tag{32}$$

which is clearly exponentially stable.

VI. Comparison between the complex and the simplified model

This section presents simulation results in order to compare the complex snake robot model given by (3) and the simplified model given by (29). Both models were implemented and simulated in *Matlab R2008b* on a laptop running *Windows XP*. The dynamics was calculated using the *ode45* solver in Matlab with a relative and absolute error tolerance of 10^{-6}.

A. Simulation parameters

We considered a snake robot with $N = 10$ links of length $l = 0.14$ m and mass $m = 1$ kg. The links of the snake robot with revolute joints had moment of inertia $J = 0.0016$ kgm^2. The friction coefficients of the complex model were set to $c_t = 0.5$ and $c_n = 3$, while the friction coefficients of the simplified model were set to $c_1 = 0.45$, $c_2 = 3$, $c_3 = 0.5$ and $c_4 = 20$. Note that defining a suitable mapping between the friction coefficients in the two models remains a topic of future work. Both models were simulated with the controller given by (31) with controller gains set to $k_p = 20$ and $k_d = 5$. The joint reference coordinates were calculated according to the motion pattern *lateral undulation*, defined in (6). The joint reference coordinates in the complex model were calculated with $\alpha = 30°$, $\omega = 70°$/s, and $\delta = 40°$, and in the simplified model with $\alpha = 0.1$ m, $\omega = 70°$/s, and $\delta = 40°$. The joint offset coordinate was set to $\phi_o = \frac{1}{6}\alpha$ in the time interval $t \in [20, 30]$ and $\phi_o = -\frac{1}{6}\alpha$ in the time interval $t \in [50, 60]$. The offset angle was set to $\phi_o = 0$ outside these two time intervals. The initial state values of both models were $(\boldsymbol{\phi}=\boldsymbol{0}, \theta=0, p_t=0, p_n=0, \boldsymbol{v}_\phi=\boldsymbol{0}, v_\theta=0, v_t=0, v_n=0)$.

B. Simulation results

The simulated motion of the CM of the snake robot with the complex and the simplified model is shown in Fig. 9(a) and Fig. 9(b), respectively. In both figures, the configuration of the snake robot is shown at $t = 10$ s, $t = 40$ s, and $t = 70$ s. The simulated orientation of the snake robot with both models is shown in Fig. 9(c). The orientation with the complex model was estimated as the average of the link angles, i.e. as $\overline{\theta} = \frac{1}{N}\sum_{i=1}^{N}\theta_i$. The orientation with the simplified model was given by θ. Fig. 9(d) and (e) show the CM velocity of the snake robot in the global x and y direction, respectively.

The simulation results indicate that the *qualitative* behaviour of the snake robot with the simplified model is similar to the behaviour with the complex model. With the chosen numerical values of the friction coefficients, we also achieved a good *quantitative* similarity between the two models. The plots corresponding to the complex model have high-frequency fluctuations that are not visible in the plots from the simplified model. This indicates that there are nonlinear components of the complex model that are not included in the simplified model. However, the similar behaviour of the two models indicate that the simplified model contains the parts of the complex model that determine the overall motion of the snake robot. This suggests that we may use the simplified model to develop general analysis and control design results that will also apply to the complex model.

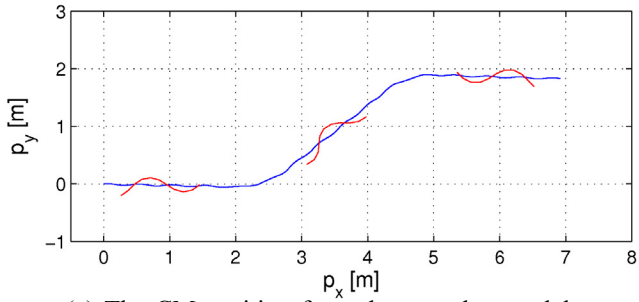

(a) The CM position from the complex model.

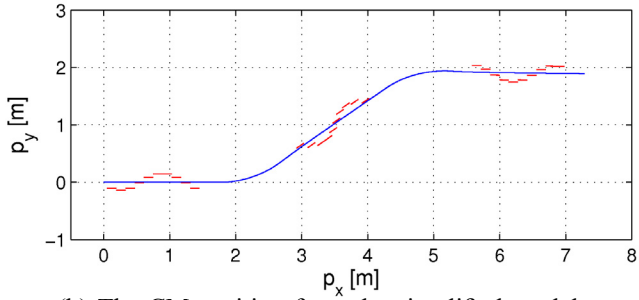

(b) The CM position from the simplified model.

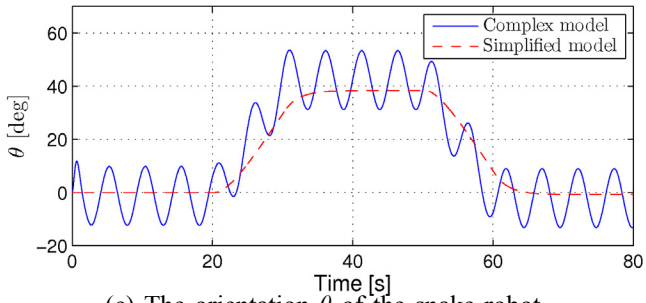

(c) The orientation θ of the snake robot.

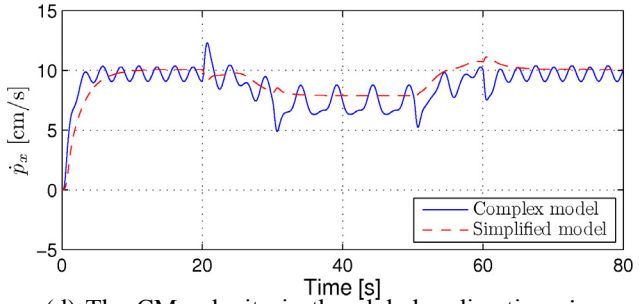

(d) The CM velocity in the global x direction, $\dot{p}_x$.

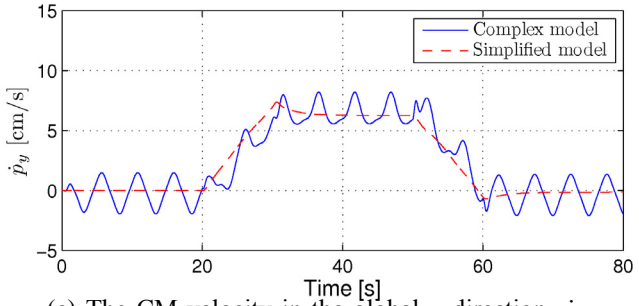

(e) The CM velocity in the global y direction, $\dot{p}_y$.

Fig. 9. Simulation results that compare the complex and the simplified model of the snake robot.

VII. Conclusions and Future Work

This paper has presented a simple model of the kinematics and dynamics of a planar, wheelless snake robot aimed at control design and stability analysis purposes. The proposed model is significantly less complex than existing models of planar snake locomotion.

The paper has presented an analysis of an existing complex snake robot model which revealed a set of essential properties that characterize the overall motion of a planar snake robot. The model proposed in this paper was developed to capture only these essential properties of snake locomotion. This approach produced a model with significantly reduced complexity compared to the original model used in the analysis. The simulation results indicated that the *qualitative* behaviour of the proposed model and the original complex model are similar, and that a *quantitative* similarity is achieved with a proper choice of numerical values of the friction coefficients in the two models.

In future work, the authors will employ the proposed model in order to develop and analyse stability of controllers for snake robot locomotion.

References

[1] J. Gray, "The mechanism of locomotion in snakes," *J. Exp. Biol.*, vol. 23, no. 2, pp. 101–120, 1946.

[2] S. Hirose, *Biologically Inspired Robots: Snake-Like Locomotors and Manipulators*. Oxford: Oxford University Press, 1993.

[3] G. Chirikjian and J. Burdick, "The kinematics of hyper-redundant robot locomotion," *IEEE Trans. Robot. Autom.*, vol. 11, no. 6, pp. 781–793, December 1995.

[4] T. Kane and D. Lecison, "Locomotion of snakes: A mechanical 'explanation'," *Int. J. Solids Struct.*, vol. 37, no. 41, pp. 5829–5837, October 2000.

[5] S. Ma, "Analysis of creeping locomotion of a snake-like robot," *Adv. Robotics*, vol. 15, no. 2, pp. 205–224, 2001.

[6] M. Saito, M. Fukaya, and T. Iwasaki, "Serpentine locomotion with robotic snakes," *IEEE Contr. Syst. Mag.*, vol. 22, no. 1, pp. 64–81, February 2002.

[7] K. McIsaac and J. Ostrowski, "Motion planning for anguilliform locomotion," *IEEE Trans. Robot. Autom.*, vol. 19, no. 4, pp. 637–625, August 2003.

[8] G. P. Hicks, "Modeling and control of a snake-like serial-link structure," Ph.D. dissertation, North Carolina State University, 2003.

[9] P. Liljebäck, Ø. Stavdahl, and K. Y. Pettersen, "Modular pneumatic snake robot: 3D modelling, implementation and control," in *Proc. 16th IFAC World Congress*, July 2005.

[10] A. A. Transeth, R. I. Leine, Ch.. Glocker, and K. Y. Pettersen, "Non-smooth 3D modeling of a snake robot with frictional unilateral constraints," in *Proc. IEEE Int. Conf. Robotics and Biomimetics*, Kunming, China, Dec 2006, pp. 1181–1188.

[11] P. Liljebäck, K. Y. Pettersen, Ø. Stavdahl, and J. T. Gravdahl, "Controllability analysis of planar snake robots influenced by viscous ground friction," in *Proc. IEEE/RSJ Int. Conf. Intelligent Robots and Systems*, 2009, pp. 3615–3622.

[12] M. Nilsson, "Serpentine locomotion on surfaces with uniform friction," in *Proc. IEEE/RSJ Int. Conf. Intelligent Robots and Systems*, 2004, pp. 1751–1755.

[13] M. Sfakiotakis and D. Tsakiris, "Biomimetic centering for undulatory robots," *The Int. Journal of Robotics Research*, vol. 26, pp. 1267–1282, 2007.

[14] K. Y. Pettersen and O. Egeland, "Exponential stabilization of an underactuated surface vessel," in *Proc. 35th IEEE conf. Decision and Control*, vol. 1, December 1996, pp. 967–972.

[15] R. Hatton and H. Choset, "Approximating displacement with the body velocity integral," in *Proc. Robotics: Science and Systems*, 2009.

[16] D. Hu, J. Nirody, T. Scott, and M. Shelley, "The mechanics of slithering locomotion," in *Proc. National Academy of Sciences, USA*, vol. 106, no. 25, 2009, p. 10081Ű10085.